Circuit Model for Resonant Cavity Mode Enabled Wireless Power Transfer

Mohsen Shahmohammadi
Disney Research, Pittsburgh
Pittsburgh, PA, 15213
mohsen.shahmoh@disneyresearch.com

Matthew J. Chabalko
Disney Research, Pittsburgh
Pittsburgh, PA, 15213
matt.chabalko@disneyresearch.com

Alanson P. Sample
Disney Research, Pittsburgh
Pittsburgh, PA, 15213
alanson.sample@disneyresearch.com

***Abstract*—Recently, a new paradigm in wireless power transfer based on cavity mode resonance has experimentally shown the ability to efficiently deliver power to multiple receivers over large 3D volumes of an enclosed metallic cavity. However, existing analytical models based on coupled mode theory and finite element simulation tools are complicated to use, relatively slow to converge, and fail to give researchers and system designers the intuition to optimize wireless power transfer performance. In this work a general circuit model for the cavity resonant wireless power system is introduced and validated against simulated and measured results. Results show an average agreement between the circuit model and measured transfer efficiency are within +/- 5%. Thus, cavity mode enabled wireless power transfer can be analyzed with an equivalent circuit model allowing for fast design iteration and a better understanding of how to optimize system performance. We used the circuit model developed herein to design a simple impedance matching network for 52 LED receivers and transferred power wirelessly to all of them simultaneously with approximately 30% efficiency, by combining two cavity modes, TE_{011} and TE_{012}. However, under optimal load condition, which requires more complicated matching circuit, a minimum efficiency of 50% can easily be achieved at the same positions, we instead here we focused on a simple and fast design solution.**

***Keywords*—Wireless power transfer, cavity resonator, circuit model, multiple receivers.**

I. Introduction

In recent years wireless power transfer (WPT) has been explored heavily both in near-field techniques such as magnetoquasistatic WPT [1], [2] and far-field techniques such as retroreflective antenna arrays [3]–[5]. MQS systems suffer low efficiency when transmitter and receiver are farther than one coil diameter apart. On the other hand, far field techniques suffer from the need for sophisticated control algorithms necessary to coordinate antenna arrays, as well as suffering from stricter power output limits that exist at the higher frequencies of far-field WPT. An alternative WPT system recently demonstrated and described in the literature uses near-field cavity modes of enclosed metal structures to enable wireless power transfer [6], [7]. This technique uses the natural resonant modes of hollow metallic cavities to transfer power wirelessly to multiple receivers contained anywhere within the chamber. Initial studies have experimentally shown power transfer efficiencies (to one or more small single turn coils) of 60–80% over large 3D volumes of the enclosed cavity. One application of cavity mode enabled WPT is the wireless recharging of multiple power tools contained in a metallic tool chest [Fig. 1(c)].

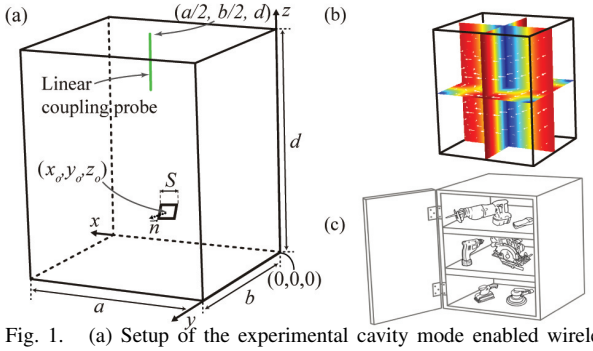

Fig. 1. (a) Setup of the experimental cavity mode enabled wireless power transfer system analyzed in this work. Probe position is shown for excitation of the TM_{110} mode. (b) Magnetic ($\vec{H}$-fields) of the TM_{110} mode. Color: $|\vec{H}|$; Red, large; Blue, small. White arrows: $\vec{H}$-field vectors. (c) Example application of cavity mode enabled WPT.

In previous work [6], coupled mode theory was used to describe the operation of the cavity mode enabled WPT system. However, this approach is unintuitive and requires a deep knowledge of the wave field patterns within the chamber. To enable new research on this topic, this work shows that the system can be abstracted by a two port network and circuit model that allows for the application of impedance matching techniques that have grown common in the WPT literature. By first measuring the impedance parameters (Z-parameters) of the cavity, and then fitting the circuit model parameters to the Z-parameters of the circuit model, a circuit model analysis based tool of cavity mode enabled WPT system is fully developed. We validate the model by comparing measured efficiencies to those predicted by the circuit model. Additionally, to highlight the power of the resultant circuit model, we use it to design an impedance matching circuit for 52 receivers that allows for powering of 52 LEDs simultaneously, and over a large volume of the experimental chamber.

II. System Analysis

A. System Topology

A typical setup depicting cavity mode enabled WPT is shown in Fig. 1(a). It shows a cavity with dimensions $a \times b \times d$, which contains a square shaped loop receiver within the chamber. The coil has side length, S, unit normal vector $\vec{n}$, and is centered at position (x_o, y_o, z_o). Wireless power transfer is accomplished via the coupling of the magnetic fields of the cavity's resonant modes to the loop receiver via magnetic induction. In this work the focus will be on three particular cavity modes, the TM_{110}, TE_{011}, and TE_{012} modes, for illustrative purposes only. Nearly identical analysis can be

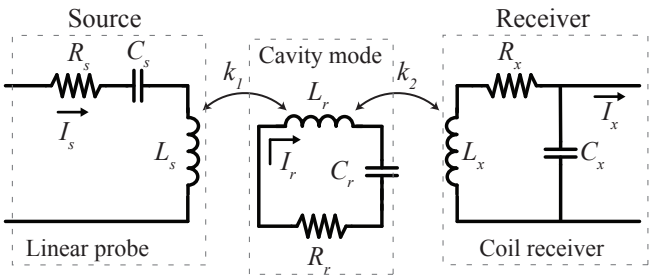

Fig. 2. Circuit topology used to model coupling from linear probe (source end) to chamber and then from chamber to receiver.

applied to other cavity modes. The magnetic field, $\vec{H}$, for the TM_{110} mode is shown in Fig. 1(b).

B. Circuit Topology

The modes supported by a metallic cavity resonator are high Quality factor modes that alternately store energy in their electric and magnetic fields. This behavior is very similar to the behavior of a lumped circuit RLC tank, and is the main motivation for seeking to describe the system in terms of simple circuit elements.

In particular, the analysis and experiments here focus on a particular mode of a rectangular cavity resonator: the TM_{110}, TE_{011}, and TE_{012} modes, which are excited by using linear monopole antennas [e.g. Fig. 1(a)]. Once the probe excites a cavity mode, the receiver can extract energy from it. Given this coupling process, a repeater type model of coupled RLC circuits is proposed here, similar to repeater models developed in the MQS WPT literature [8]. In general, the system can be represented by a simple two-port model and subsequent circuit. In this case, we choose to work with two-port impedance parameters (or Z-parameters) since they give physical insight into the impedances looking into the source end (the input to the linear probe) and the receiver end (square shaped loop receiver). Figure 2 shows the system represented as a repeater type circuit. The transmitter (linear coupling probe) has an effective resistance, capacitance, and inductance, R_s, C_s, and L_s, respectively. Similarly, the receiver coil is modeled with effective R_x, C_x, and L_x. Lastly, the cavity mode is modeled as a resonant series RLC circuit with R_r, C_r, and L_r. The coupling between linear probe and cavity mode is modeled as a transformer via the mutually coupled inductors L_s and L_r, with coupling coefficient k_1. Similarly, the coupling from cavity mode to receiver is modeled via the mutually coupled inductors L_r and L_x, with coupling coefficient, k_2.

C. Circuit Analysis

Given the above circuit model, the task becomes verification. In this case, the experimentally measured Z-parameters of the system will be fitted to the circuit model by adjusting the unknown resistances, capacitances, and inductances of Fig. 2 such that the measured Z-parameters match well with the analytic Z-parameters of Fig. 2 across a frequency band that spans above and below the chamber's resonant frequency for a particular resonant mode. In this case, a curve fitting routine will be used to fit experimental data to the circuit model as depicted in Fig. 3.

The analytic expressions for the various real and imaginary parts of the system Z-parameters can be obtained by circuit analysis of the source and receiver ports of Fig. 2. The parameter extraction routine is then implemented using unconstrained nonlinear optimization (Matlab's "fminsearch()") to minimize the difference between the measured Z-parameters and the analytic model for the same Z-parameters across the entire measured frequency range by varying the degrees of freedom available from the unknown quantities of Fig. 2. The algorithm tries to obtain a value as close to unity as possible for the r^2 curve-fitting correlation coefficient.

TABLE I. INITIAL GUESS VALUES FOR CAVITY CIRCUIT MODEL

Circuit Parameter	Initial Value
L_r	$\mu_o k^2 V$
C_r	$\frac{\epsilon_o}{k^4 V}$
R_r	$\frac{1}{Q_C}\sqrt{\frac{L_r}{C_r}}$

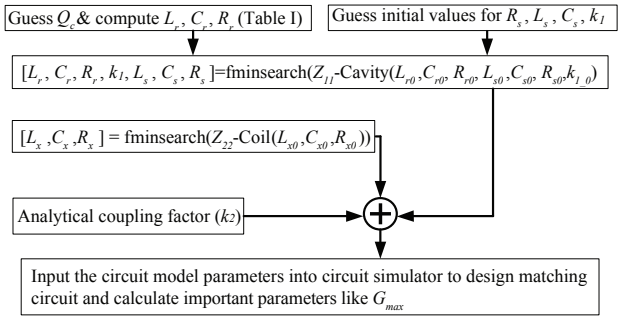

Fig. 3. Circuit parameter extraction and verification routine.

The parameter extraction process is done in two stages. First, the Z_{11}-parameter of the linear probe coupling to the chamber alone is measured and fit in isolation. Next, the impedance looking into the coil alone (outside the chamber) is measured. In terms of impedance parameters, this measurement yields the Z_{22}-parameter. Fitting these two (Z_{11} and Z_{22}) independent measurements will result in R_s, C_s, L_s, k_1, R_r, L_r, C_r, R_x, C_x, and L_x. The initial values (ie.e. the initial inputs to the numeric optimization routine) for the circuit model are listed in Table. I, where μ_o and ϵ_o are the permeability and permittivity of air, V is the cavity volume, k is the cavity mode wave-number (CMWN) for a particular cavity mode, and Q_C is the cavity's quality factor (Q-factor). The initial guess of C_x and L_x for receiver coil are made by solving the $\Im Z_{22}$ assuming $R_x = 0$ at two different frequencies from measurement. Then, R_x is found by solving $\Re Z_{22}$ using C_x and L_x. The remaining parameter k_2 is a variable that will be obtained analytically later. Lastly, all parameters are fed into an RF circuit simulator and maximum available power gain (the upper bound on power transfer efficiency assuming a perfectly lossless and biconjugate impedance matching network), denoted as G_{max} in this work, is calculated. The entire process just described is

TABLE II. SHOWS CIRCUIT PARAMETER RESULTS AND r^2 CORRELATION COEFFICIENT.

Cavity Mode	TM110	TE011	TE012
Ckt. Parameter	Value	Value	Value
R_s	0.648 Ω	0.975 Ω	0.2981 Ω
L_s	90.77 nH	59.20 nH	107.90 nH
C_s	5.254 pF	5.892 pF	4.210 pF
R_r	54.58 Ω	9.99 Ω	63.70 Ω
L_r	41.70 μH	35.54 μH	68.36 μH
C_r	29.78 fF	40.53 fF	9.86 fF
Q_r	685	2960	1305
k_1	0.1356	0.1800	0.1145
Probe Length	33 cm	28.3 cm	25.2 cm
f_0	142.8 MHz	132.6 MHz	193.78 MHz
CMWN(k)	3.0212	2.7981	4.0844
r^2 coefficient (Z_{11})	0.9998	0.9999	0.9999

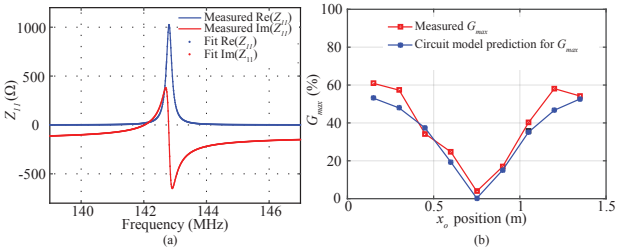

Fig. 4. (a) shows the measured Z_{11}-parameters of the cavity mode TM110 and the fitted Z-curves that result after fitting. (b) Upper bound on system efficiency, G_{max} for both experiment (red curve) and those computed by simulating the circuit model of Fig. 2 with parameters as given in Table I and the theoretically predicted value of k_2 derived analytically.

outlined in the flow chart of Fig.3.

III. Experimental Results

To test the circuit model we built an Aluminum cavity with dimensions $a = 1.52$ m, $b = 1.42$ m, and $d = 1.83$ m. The cavity resonant frequency for the TM_{110} mode is around 143 MHz as measured with a Vector Network Analyzer (VNA), with Q-factor of 685. Similarly, we built a square shaped copper loop receiver that had side length S=7.6 cm and $\vec{n} = \vec{a}_y$, with varied position x_o = 15–135 cm, and fixed $y_o = b/2$, z_o=17 cm. Since the magnetic flux density is y-directed along these positions [Fig. 1(b)], the receiver couples strongly to the cavity mode via the magnetic fields. Lastly, the linear coupling probe was mounted at the middle of the ceiling panel of the cavity to efficiently excite the TM_{110} mode. Since efficiency is likely the most important figure of merit in WPT systems, the verification experiment here seeks to ascertain the predictive ability of the proposed circuit model. Thus, what is sought is a comparison of predicted efficiency versus measured efficiency.

Experimentally, this was tested by tuning the resonant frequency of the square shaped coil to 143 MHz using a lumped capacitor. This is near the chamber's resonant frequency, at the minimum of the reflection coefficient, S_{11} as viewed from the source or receiver sides. A small 2.54 cm diameter copper loop probe was then brought in proximity (within 1 mm) to the square loop and used to magnetically couple out of it. This loop is the impedance matching "mini-loop" familiar from MQS wireless power transfer systems, [9], and is the method used for effectively impedance matching the coil to the chamber.

After tuning, the position of the receiver was varied as mentioned above and the Z-parameters were measured with a vector network analyzer (VNA). Ideally, the tuning process would lead to a fully bi-conjugate impedance matched system and optimal efficiency. This, however, is not always the case since the receiver is moved around the chamber yielding variations in coupling coefficient, k_2; thus, some power is lost to reflections. Due to this fact the efficiency metric we use here is one that seeks an *upper bound* on the efficiency that could have been achieved assuming a lossless and perfect impedance matching network. In the literature this efficiency figure of merit is often referred to as G_{max}. In terms of system two-port Z-parameters, it is computed from [10]:

$$G_{max} = \frac{\chi}{(1+\sqrt{1+\chi})^2}. \tag{1}$$

where χ is defined as

$$\chi = \frac{|Z_{21}|^2}{\Re Z_{11}\Re Z_{22} - \Re Z_{21}^2}, \tag{2}$$

Given this definition then, at 143 MHz the coupled system (i.e. the tuned receiver and linear probe are both in the chamber and attached to ports I and II of the VNA, respectively) Z-parameters are measured and then used in (1) and (2) to compute an upper bound on efficiency.

Having obtained efficiency experimentally, attention turns to computing it based on the circuit model of Fig. 2. The same G_{max} value at 143 MHz was extracted via simulation using the commercial RF circuit simulator software Advanced Design System (ADS) by Keysight. The parameters used for the resistances, capacitances, and inductances of the circuit of Fig. 2 as extracted using the method outlined in Sec. II-C from measured Z-parameters of system are shown in Table II. The circuit model parameters for two additional modes, TE_{011} and TE_{012}, are also shown. The extracted parameters for the square shape coil are $R_x = 2.745\Omega$, $L_x = 208.59nH$ and $C_x = 2.722pF$. The correlation coefficient (r^2) showing the quality of the fit for each of the measured Z-parameters ($\Re Z_{11}$, $\Im Z_{11}$, $\Re Z_{22}$, $\Im Z_{22}$) is larger than 0.9998 for all three modes. As an example, the Z_{11}-parameter versus frequency obtained from the circuit model is compared against measurement for TM_{110} mode in Fig. 4 (a).

To simulate the variation in position of the receiver within the chamber, it is necessary to know the coupling coefficient between chamber and receiver, k_2. This value was computed first by computing the coupling rate, κ, via the method introduced and detailed in [6]. In this way, the coupling rate is then found to be:

$$\kappa = \frac{2\sin\left(\frac{\pi\, y_o}{b}\right)\cos\left(\frac{\pi\, x_o}{a}\right)\sin\left(1/2\,\frac{\pi\, S}{a}\right) S}{\sqrt{L_2}\sqrt{\frac{\pi^2(a^2+b^2)d}{\mu_o\,{\omega_o}^2 ba}}} \tag{3}$$

where ω_o is the chamber's resonant frequency for the TM_{110} mode. The relationship that transforms κ to k_2 necessary for inclusion in the circuit model is then given by [11], $k_2 = \frac{2\kappa}{\omega_o}$.

Finally, each of the *computed* k_2 values obtained from evaluating equations (3) and $k_2 = \frac{2\kappa}{\omega_o}$, for each of the varied positions, x_o, of the receiver were then used in an ADS circuit model simulation to extract G_{max}. The simulated and measured values are plotted in Fig. 4 (b). The results show good agreement between the values computed via the circuit analysis technique and those actually measured. The fact that the measured values are larger than the values from circuit simulation is likely due to the fact that there is also some level of coupling via the electric field of the chamber to the coil [12], a mechanism not accounted for in the circuit model. Additionally, the presence of the metallic coaxial cable, which is attached to the receiver inside the chamber for measuring efficiency also perturbs the fields of the pure TM_{110} mode, yielding field patterns and strengths that differ somewhat from the perfect analytical case. The predictive capabilities of the circuit model are nonetheless of value since the circuit model is a strong abstraction of the actual power transfer mechanism, which is the spatially varying magnetic fields of the TM_{110} mode. Typically, circuit model analysis applies when the physical elements are much smaller than a wavelength, but in this case we have shown that even though the dimensions of the cavity are comparable to a wavelength at 140 MHz, circuit model analysis still can capture all the most important phenomena of cavity mode enabled wireless power transfer.

The parameters we have extracted can be inserted into a circuit simulator and then analyzed from a circuit perspective.

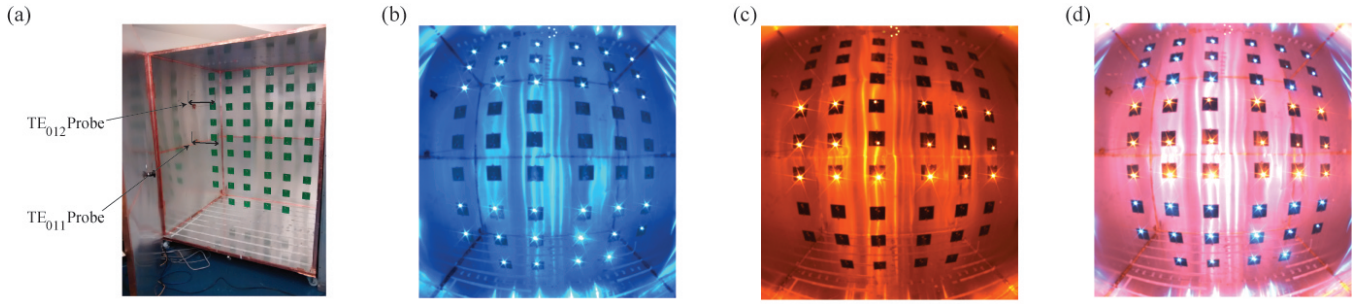

Fig. 5. (a) Aluminum chamber with 52 LED circuits at $y_o = b/2$ plane. LEDs are powered by (b) TE_{011} mode, (c) TE_{012} mode, (d) both modes simultaniously.

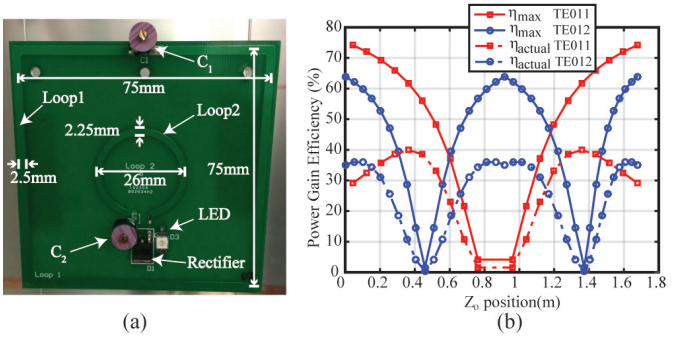

Fig. 6. (a) The implemented receiver is depicted with the marked dimensions.(b) Upper bound on system efficiency, η_{max} and actual efficiency, η_{actual}, are plotted for TE011 and TE012 modes on $y_o = b/2$ plane as the receiver coil is moved from bottom to top of the chamber parallel to $y_o = 0$.

For instance, once the circuit parameters are extracted, a tuning network on the transmitter and receiver end can be designed such that power is optimally transferred between source and load ends for any given geometric configuration of the chamber, coupling probe, and receiver. In this way it provides a familiar and convenient tool for analyzing and optimizing cavity mode enabled wireless power transfer networks.

Finally, as a demonstration of the circuit model's utility, we designed and fabricated the square loop and the impedance-matching mini-loop, described earlier in this section on FR-4 PCB as shown in Fig. 6 (a). The equivalent circuit model of the receiver circuit is very similar to the circuit model of the source inductively coupled into the cavity using linear probe shown in Fig. 2, as detailed in [13]. So we used the same method to extract the circuit parameters of PCB receivers. The whole coupled system, i.e. cavity-to-receiver, is simulated in Advanced Design System (ADS) using the analytical values for coupling coefficient between chamber and receiver. η_{max} and η_{actual} are plotted for the $y_o = b/2$ plane for variations along axis z_o in Fig. 6 (b). It shows that an actual efficiency of 30-40% is achieved using a simple matching circuit when the receiver is tuned for the TE_{012} mode and positioned near the middle of z-axis. Similarly, the TE_{011} can be used when the receiver is near the top or bottom of the chamber and still achieve 30% efficiency or greater. Although, a much higher efficiency can be achieved using more complicated matching circuit, we focused on a simple and easy to implement solution here. Finally, 52 of these receiver boards connected to rectifier/LED loads, consuming normally 350-500 mW, are wirelessly powered using 50 Watts input power. Fig. 5 (b) shows powering LEDs near the top/bottom of the chamber using TE_{011} mode. Fig. 5 (c) shows LEDs near the middle of the chamber powered by TE_{012} mode. LEDs are powered at both locations using the two modes together *simultaneously* as shown in Fig. 5 (d). The blue LEDs had impedance matching networks designed for the TE_{011} mode using the circuit theory developed in this work, and the red LEDs similarly had impedance matching networks designed for the TE_{012} mode. Thus, by using two modes and impedance matching networks appropriate for each mode, we are able to cover the entire middle $y-z$ plane of the chamber.

IV. Conclusion

A circuit model for analyzing cavity mode enabled WPT systems has been hypothesized and tested. The results show that the model can be fit well to the circuit model proposed via a high quality r^2 correlation coefficient. The results offer a convenient and familiar tool to analyze. Now, all the tools developed for impedance matching and optimization of MQS WPT networks now become available to a designer in cavity mode enabled WPT systems. Lastly, we used the circuit model to design a simple matching network for multiple receivers (52 LED circuits) and powered all of them simultaneously, highlighting the utility of this approach.

References

[1] A. Kurs, A. Karalis, R. Moffatt, J. D. Joannopoulos, P. Fisher, and M. Soljacic, "Wireless power transfer via strongly coupled magnetic resonances," *Science*, vol. 317, no. 5834, pp. 83–86, 2007.

[2] A. P. Sample, B. H. Waters, S. T. Wisdom, and J. R. Smith, "Enabling seamless wireless power delivery in dynamic environments," *Proc. of the IEEE*, vol. 101, no. 6, pp. 1343–1358, June 2013.

[3] C. C. Capelli, et al., "Recharging method and apparatus," U.S. Patent No. 7,373,133. (13 May 2008).

[4] W. C. Brown, "The history of power transmission by radio waves," *IEEE Trans. Microw. Theo. Tech.*, vol. 32, no. 9, pp. 1230–1242, 1984.

[5] S. Korhummel, A. Rosen, and Z. Popovic, "Over-moded cavity for multiple-electronic-device wireless charging," *IEEE Trans. Microw. Theo. Techn.*, vol. 62, no. 4, pp. 1074–1079, April 2014.

[6] M. J. Chabalko and A. P. Sample, "Resonant cavity mode enabled wireless power transfer," *Applied Physics Letters*, 105.24 (2014): 243902.

[7] M. J. Chabalko and A. P. Sample, "Three-dimensional charging via multimode resonant cavity enabled wireless power transfer," *IEEE Trans. Ind. Elec.*, vol. 30, no. 11, pp. 6163–6173, 2015.

[8] D. Ahn and S. Hong, "A study on magnetic field repeater in wireless power transfer," *IEEE Trans. Ind. Electrons.*, vol. 60, no. 1, pp. 360–371, 2013.

[9] D. S. Ricketts, M. J. Chabalko, and A. Hillenius, "Experimental demonstration of the equivalence of inductive and strongly coupled magnetic resonance wireless power transfer," *Applied Physics Letters*, 102.5 (2013): 053904.

[10] M. Zargham and P. G. Gulak, "Maximum achievable efficiency in near-field coupled power-transfer systems," *IEEE Trans. Biomed. Circuits Syst.*, vol. 6, no. 3, pp. 228–245, 2012.

[11] E. Bou Balust, E. J. Alarcon Cot, and J. L. Gutierrez Cabello, "A comparison of analytical models for resonant inductive coupling wireless power transfer," in *PIERS 2012, Moscow*, 2012, pp. 689–693.

[12] M. J. Chabalko and A. P. Sample, "Electric field coupling to short dipole receivers in cavity mode enabled wireless power transfer," in *Symposium on Antennas and Propag.*, 2015, pp. 410–411.

[13] D. Barrick, "Miniloop antenna operation and equivalent circuit," *IEEE Trans. Antennas and Propag.*, vol. 34, no. 1, pp. 111–114, Jan 1986.